

Dispersion Distance and the Matter Distribution of the Universe in Dispersion Space

Kiyoshi Wesley Masui

Department of Physics and Astronomy, University of British Columbia, Vancouver, British Columbia, V6T 1Z1, Canada and Canadian Institute for Advanced Research, CIFAR Program in Cosmology and Gravity, Toronto, Ontario, M5G 1Z8, Canada

Kris Sigurdson

Department of Physics and Astronomy, University of British Columbia, Vancouver, British Columbia, V6T 1Z1, Canada

We propose that “standard pings”, brief broadband radio impulses, can be used to study the three-dimensional clustering of matter in the Universe even in the absence of redshift information. The dispersion of radio waves as they travel through the intervening plasma can, like redshift, be used as a cosmological distance measure. Because of inhomogeneities in the electron density along the line of sight, dispersion is an imperfect proxy for radial distance and we show that this leads to calculable dispersion-space distortions in the apparent clustering of sources. Fast radio bursts (FRBs) are a new class of radio transients that are the prototypical standard ping and, due to their high observed dispersion, have been interpreted as originating at cosmological distances. The rate of fast radio bursts has been estimated to be several thousand over the whole sky per day and, if cosmological, the sources of these events should trace the large-scale structure of the Universe. We calculate the dispersion-space power spectra for a simple model where electrons and FRBs are biased tracers of the large-scale structure of the Universe and we show that the clustering signal could be measured using as few as 10 000 events. Such a survey is in line with what may be achieved with upcoming wide-field radio telescopes.

Introduction.—The clustering of matter on large scales has been heralded as the next great probe of the Universe after the cosmic microwave background (CMB). The large-scale structure, in principle, contains far more information than the CMB because it can be studied in three dimensions. Traditionally, the redshift of spectral lines of “standard atoms”, caused by the Hubble flow, has been employed to measure radial distance and provide the third dimension. Such redshift surveys have now aggregated the positions of millions of galaxies into three dimensional density maps, exposing a rich structure of clusters, filaments, walls, and voids.

However, redshift is not the only measure of radial distance. Standard candles and standard rulers can be used to estimate distance using brightness and angular size, respectively. In the same way a “standard ping”, a brief broadband radio impulse, can be used to measure dispersion through the characteristic wavelength-squared delay of electromagnetic signals. The dispersion is proportional to the amount of plasma along the line of sight and can thus be used to estimate radial distance. This technique, routinely used for pulsars in the Galaxy, can be used to define a *dispersion distance* to cosmological sources.

Dispersion is readily measured from fast radio bursts (FRBs), a new class of millisecond duration radio transients first reported by Lorimer *et al.* [1], which are the archetype of a standard ping. Ten such bursts have been reported to date [2–7], and the total event rate has been estimated to be $3.3_{-2.5}^{+5} \times 10^3$ per sky per day [8]. Dispersion is characterized by a line-of-sight integral of the free electron density known the dispersion measure (DM). FRB events are observed to have dispersion measures of order ~ 1000 pc/cm³, greatly in excess of the galactic expectation of order ~ 100 pc/cm³ (depending on galactic latitude) [9]. They thus appear to be of extragalactic origin, with their dispersion produced either by the intergalactic medium, associated with structure along line

of sight [3], or the environment of the source [10–12]. If the dispersion is dominated by electrons along the line of sight, then the average dispersion–distance relation can be modeled [13–15] and the sources appear to be at cosmological distances of order gigaparsecs. Such cosmological distances permit the study of the clustering of FRB sources in three dimensions, with an expectation that these events trace the large-scale structure of the Universe on linear scales. We note that while our discussion here is framed in terms of FRBs, other bright radio transients that fluctuate on time scales shorter than the typical differential lag of ~ 1 s/100 MHz might also be useful as standard pings.

Neither redshift nor dispersion are perfect proxies for radial distance. Redshifts are systematically biased by the peculiar velocities of objects relative to the Hubble flow. This leads to additional apparent clustering in redshift space which was first calculated by Kaiser [16] using linear theory. Similarly, as we show here, distance estimates from dispersion will be biased by inhomogeneities in the electron density [17], again leading to additional apparent clustering of sources in dispersion space. In this Letter we calculate these dispersion-space distortions and consider the detectability of the signal by upcoming surveys.

Clustering in dispersion space.—The dispersion measure of a signal observed in some angular direction \hat{n} and originating from comoving radial distance χ is

$$\text{DM}(\hat{n}, \chi) = \int_0^\chi d\chi' a(\chi')^2 n_e(\hat{n}\chi', \chi'). \quad (1)$$

Here $n_e(\vec{x}, \chi)$ is the free electron density as a function of location and conformal time. Note that we use χ as our radial distance and time coordinate, as opposed to redshift. We model the cosmological electron density as containing a homogeneous part and perturbations, $n_e(\vec{x}, \chi) =$

$\bar{n}_e(\chi) [1 + \delta_e(\vec{x}, \chi)]$. The dispersion measure is thus

$$\text{DM}(\hat{n}, \chi) = \int_0^\chi d\chi' a(\chi')^2 \bar{n}_e(\chi') [1 + \delta_e(\hat{n}\chi', \chi')]. \quad (2)$$

Dispersion space is the three-dimensional coordinates, \vec{x}_s , inferred from the dispersion measure assuming that the electrons are homogeneous. This only affects the radial coordinate such that $\vec{x}_s = \hat{n}\chi_s$, with χ_s defined by the equation

$$\text{DM}(\chi_s) = \int_0^{\chi_s} d\chi' a(\chi')^2 \bar{n}_e(\chi'). \quad (3)$$

Combining the above equations (keeping only terms first order in the density perturbations), we find that

$$\frac{d\chi_s}{d\chi} = 1 + \delta_e(\hat{n}\chi, \chi), \quad (4)$$

and thus

$$\chi_s - \chi = \int_0^\chi d\chi' \delta_e(\hat{n}\chi'). \quad (5)$$

We wish to relate the density of a tracer, f , measured in dispersion space to its density in real space. We follow the derivation in Kaiser [16] of the redshift-space distortions. Start by noting that the total number of tracers in a volume element is the same in both spaces:

$$n_{fs}(\vec{x}_s) d^3\vec{x}_s = n_f(\vec{x}) d^3\vec{x}. \quad (6)$$

We split the density into a homogeneous part plus perturbations,

$$\bar{n}_{fs}(\chi_s) [1 + \delta_{fs}(\vec{x}_s)] d^3\vec{x}_s = \bar{n}_f(\chi) [1 + \delta_f(\vec{x})] d^3\vec{x}. \quad (7)$$

Averaged over the sky, $\langle \chi_s \rangle = \chi$, and thus the background density should be the same in dispersion space as in real space,

$$\bar{n}_{fs}(\chi) = \bar{n}_f(\chi). \quad (8)$$

Therefore,

$$\bar{n}_{fs}(\chi_s) = \bar{n}_f(\chi) + (\chi_s - \chi) \frac{d\bar{n}_f}{d\chi} \quad (9)$$

$$= \bar{n}_f(\chi) + \frac{d\bar{n}_f}{d\chi} \int_0^\chi d\chi' \delta_e(\hat{n}\chi'). \quad (10)$$

The Jacobian in spherical coordinates is

$$\left| \frac{d^3\vec{x}}{d^3\vec{x}_s} \right| = \frac{d\chi}{d\chi_s} \frac{\chi^2}{\chi_s^2} \quad (11)$$

$$\approx 1 - \delta_e - \frac{2}{\chi} \int_0^\chi d\chi' \delta_e(\hat{n}\chi'). \quad (12)$$

Substituting Eqs. 10 and 12 into Eq. 7, we obtain

$$\delta_{fs} = \delta_f - \delta_e - \left(\frac{1}{\bar{n}_f} \frac{d\bar{n}_f}{d\chi} + \frac{2}{\chi} \right) \int_0^\chi d\chi' \delta_e(\hat{n}\chi'). \quad (13)$$

In the above equation, the $-\delta_e$ term is most analogous to the Kaiser redshift-space distortions. It is a dilution of tracers in dispersion space due to an excess of electrons between the tracers. However we note that this term is isotropic in contrast to the Kaiser term. This is because any wave vector electron perturbation causes dispersion-space distortions, whereas the radial velocities that cause redshift-space distortions are only sourced by perturbations with radial wave vectors.

The $\frac{1}{\bar{n}_f} \frac{d\bar{n}_f}{d\chi}$ term arises because the misinterpretation of the radial distance causes the observed tracer density to be compared to the wrong background density. The $\frac{2}{\chi}$ term is caused by a misinterpretation of angular distances when the radial distance is mismeasured. In both cases, analogous terms are, in principle, present in redshift space but are negligible. Because radial velocities are only sourced by modes with a large radial wave vector, there is near perfect cancellation along the line of sight, and thus there is very little net error in the radial distance.

For brevity in the following sections, we define the coefficient of the integral term as

$$A(\chi) \equiv \frac{1}{\bar{n}_f} \frac{d\bar{n}_f}{d\chi} + \frac{2}{\chi}. \quad (14)$$

Large-scale structure is usually studied through its two-point statistics, most commonly the power spectrum, $P(k)$. Unlike the redshift-space distortions, Eq. 13 does not have a simple form in harmonic space. The equation's third term couples harmonic modes, and thus the two-point statistics cannot be phrased as a simple power spectrum. We will instead use $C_\ell^{ss}(\chi, \chi')$, which is the cross-correlation angular power spectrum of the dispersion-space overdensity, on shells at χ and χ' :

$$C_\ell^{ss}(\chi, \chi') = \int d\Omega d\Omega' Y_{\ell m}(\hat{n}) Y_{\ell m}^*(\hat{n}') \langle \delta_{fs}(\hat{n}\chi) \delta_{fs}(\hat{n}'\chi') \rangle. \quad (15)$$

The first two terms in Eq. 13 are stationary. For stationary, isotropic tracers x and y , we have $\langle \delta_x(\vec{k}, \chi) \delta_y(\vec{k}', \chi) \rangle = (2\pi)^3 \delta^3(\vec{k} - \vec{k}') P_{xy}(k, \chi)$. If, for a moment, we ignore structure evolution, the angular cross-power spectrum of such tracers is

$$C_\ell^{xy}(\chi, \chi') = \frac{2}{\pi} \int_0^\infty dk k^2 j_\ell(k\chi) j_\ell(k\chi') P_{xy}(k). \quad (16)$$

In reality the power spectrum evolves on the order of a Hubble time. The angular cross correlations will be very small unless χ and χ' are within a few correlation lengths of one another, roughly a hundred megaparsecs. The evolution of the power spectrum is negligible over these time differences, which leads to a straightforward way to include the evolution:

$$C_\ell^{xy}(\chi, \chi') \approx \frac{2}{\pi} \int_0^\infty dk k^2 j_\ell(k\chi) j_\ell(k\chi') P_{xy}(k, (\chi + \chi')/2), \quad (17)$$

$$|\chi - \chi'| \ll 1/aH.$$

The third term in Eq. 13 is not stationary but is an integral over the stationary field δ_e . Define δ_d as

$$\delta_d(\hat{n}\chi) \equiv \int_0^\chi d\chi' \delta_e(\hat{n}\chi'). \quad (18)$$

It is straightforward to show that

$$C_\ell^{dd}(\chi, \chi') = \frac{2}{\pi} \int_0^\chi d\chi'' \int_0^{\chi'} d\chi''' \int_0^\infty dk k^2 j_\ell(k\chi'') j_\ell(k\chi''') P_{ee}(k, (\chi'' + \chi''')/2). \quad (19)$$

Finally, C_ℓ^{ss} will contain cross terms between the stationary terms and the integral terms. These will have the form

$$C_\ell^{dx}(\chi, \chi') = \frac{2}{\pi} \int_0^\chi d\chi'' \int_0^\infty dk k^2 j_\ell(k\chi'') j_\ell(k\chi') P_{ex}(k, (\chi' + \chi'')/2). \quad (20)$$

Assembling all of these expressions with the proper coefficients, we have

$$\begin{aligned} C_\ell^{ss}(\chi, \chi') &= \frac{2}{\pi} \int_0^\infty dk k^2 j_\ell(k\chi) j_\ell(k\chi') P_{[ff+ee-2ef]}(k, (\chi + \chi')/2) \\ &+ \frac{2}{\pi} A(\chi) A(\chi') \int_0^\chi d\chi'' \int_0^{\chi'} d\chi''' \int_0^\infty dk k^2 j_\ell(k\chi'') j_\ell(k\chi''') P_{ee}(k, (\chi'' + \chi''')/2) \\ &+ \frac{2}{\pi} A(\chi) \int_0^\chi d\chi'' \int_0^\infty dk k^2 j_\ell(k\chi'') j_\ell(k\chi') P_{[ee-fef]}(k, (\chi' + \chi'')/2) \\ &+ \frac{2}{\pi} A(\chi') \int_0^{\chi'} d\chi'' \int_0^\infty dk k^2 j_\ell(k\chi'') j_\ell(k\chi) P_{[ee-fef]}(k, (\chi + \chi'')/2). \end{aligned} \quad (21)$$

Here, expressions such as $P_{[ff+ee-2ef]}$ are shorthand for $P_{ff} + P_{ee} - 2P_{ef}$.

Equation 21 can be simplified substantially by adopting the small angle and Limber approximations [18–20]. The small angle approximation eliminates the k integral over spherical Bessel functions, replacing it with a Fourier transform, and is valid for $\ell \gg 1$. The Limber approximation assumes that only modes with a small radial component of their wave vector contribute to the radial integrals and is valid if the power spectra evolve slowly compared to the correlation length [21] (which has already been assumed). With these approximations, we have

$$\begin{aligned} C_\ell^{ss}(\chi, \chi') &\approx \\ &\frac{1}{\bar{\chi}^2} \int_{-\infty}^\infty \frac{dk_\parallel}{(2\pi)} e^{ik_\parallel(\chi - \chi')} P_{[ee+ff-2ef]}(\sqrt{k_\parallel^2 + \nu^2/\bar{\chi}^2}, \bar{\chi}) \\ &+ A(\chi) A(\chi') \int_0^{\chi_{\min}} d\chi'' \frac{1}{\chi''^2} P_{ee}(\nu/\chi'', \chi'') \\ &+ \frac{A(\chi_{\max})}{\chi_{\min}^2} P_{[ee-ef]}(\nu/\chi_{\min}, \chi_{\min}), \end{aligned} \quad (22)$$

where $\nu \equiv \ell + 1/2$, $\chi_{\min} \equiv \min(\chi, \chi')$, and $\chi_{\max} \equiv \max(\chi, \chi')$. We have found that these approximations are accurate to within 3% at $\ell \gtrsim 10$ and use this form for the remainder of the Letter. In the above equation, we dub the three terms the “local”, “integral” and “cross” terms, respectively, and we will refer to them as such henceforth.

Modelling and measurement.—The second term in Eq. 22

is an integral that mixes many spatial scales: small scales from smaller radial distance and larger scales from greater distances. The mixing of scales complicates the interpretation of measurements since structure formation on scales smaller than ~ 10 Mpc/ h is nonlinear and hard to model. A similar issue exists in the field of weak gravitational lensing, where the formula for the shear angular power spectrum has a similar form. In lensing, a kernel in the line-of-sight integral arising from geometric effects suppresses the contribution from small distances, partially alleviating the issue.

However, the lack of a kernel simplifies tomography—the use of sources at multiple redshifts to unmix spatial scales. Lensing tomography is inexact because the kernel’s shape depends on the source redshift, thus reweighting the line-of-sight integral. In contrast, the integrand in the dispersion-space integral term is completely independent of the limit of integration, meaning contributions from different parts of the line of sight (and thus different spatial scales) can be separated exactly. We leave a study of the potential of dispersion-space tomography to future work. To avoid our results being sensitive to the hard-to-model small scales, we assume that the contribution to the integral term from radial distances $\chi'' < 500$ Mpc/ h are well measured by the correlations with these radial slices. We thus ignore contributions to the integral term from below this distance and neglect the information from these slices in our sensitivity measurements. The smallest spatial scale that contributes to our plotted angular power spectra out to $\ell = 1000$ is thus $k = 2 h/\text{Mpc}$.

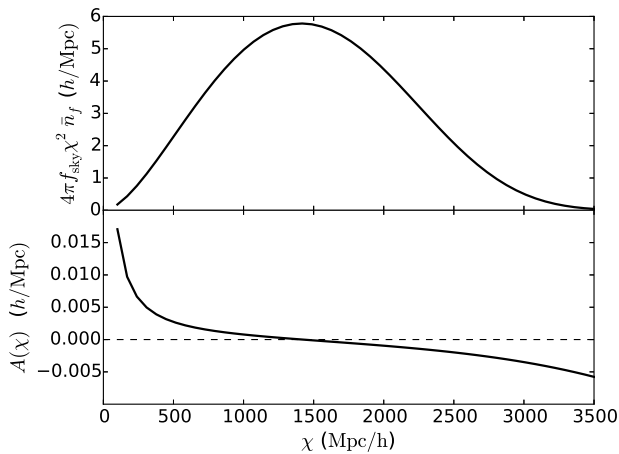


FIG. 1. (Top) Comoving density of sources in toy model, as described in text. Normalization is such that the survey has a total of 10 000 FRB events. (Bottom) Resulting coefficient $A(\chi)$ as given in Eq. 14.

For plotting the dispersion-space power spectra, we use a toy model for the electron and FRB clustering that assumes both are biased tracers of the dark matter: *i.e.* $P_{xy}(k) = b_x b_y P(k)$. We calculate the time dependant dark-matter power spectrum using CAMB, using the integrated HALOFIT to approximate the nonlinear evolution. We assume that the electron bias is $b_e = 1$, which should be true on large scales due to the approximate conservation of free electrons. The bias of FRB sources is unconstrained by data and we choose it to be $b_f = 1.3$, roughly the value for star forming galaxies at the relevant redshifts [22] and providing reasonable contrast to the electrons. The coefficient $A(\chi)$ depends on the density of detected FRB sources, $\bar{n}_f(\chi)$. We use a simple model where all events above a fixed flux are detected, the intrinsic luminosity function has the form from Schechter [23] with index -1 , and events at the cutoff of the luminosity function and at a radial distance of $\chi = 2350 \text{ Mpc}/h$ are at the flux detection threshold. This source density is shown in Fig. 1 with the resulting dispersion-space power spectrum in Fig. 2.

The amplitudes of the local and cross terms depend on the difference between the electron bias and the highly uncertain FRB bias, and the sign of the cross term depends on which of these is larger. However, since the integral term dominates for most radial distance pairs, our final sensitivity estimates are largely unaffected by this uncertainty (as shown below). In a high-precision survey, the sensitivity of the cross and local terms to the difference in the biases may help break measurement degeneracies, while sign changes of terms as a function of radial distance are a signature of bias evolution.

In a real survey, measurement of the dispersion-space clustering will be complicated by extra contributions to the dispersion. First, all signals must pass through the Milky Way’s galactic disk, halo, and local environment. However, the resulting dispersion is only a single function of \hat{n} which presumably can be well measured. As such, it should be possible

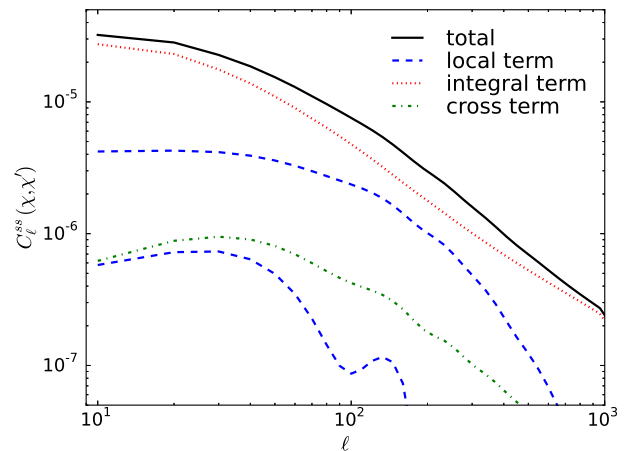


FIG. 2. Terms in the dispersion-space cross-correlation angular power spectrum. All terms are evaluated at $\bar{\chi} = 2000 \text{ Mpc}/h$ and $\chi - \chi' = 10 \text{ Mpc}/h$, except the lowest most local term curve, which is for $\chi - \chi' = 50 \text{ Mpc}/h$. While the other two terms are highly insensitive to the separation of the radial slices, the local term drops rapidly with separation.

to subtract the local contribution, as was done in Dolag *et al.* [9], and this is unlikely to be a limiting obstacle.

Perhaps more concerning is the dispersion from the source’s immediate environment as well as the halo in which it resides. These electrons will presumably be clustered around the source on scales far smaller than the survey resolution and are thus not accounted for in the $\delta_e - \delta_f$ correlations included in the above formalism. This will have a mean contribution, which is common to all sources and which may be epoch dependant, that will modify the mean dispersion–distance relation. This will need to be calibrated in some way or else fit with nuisance parameters during parameter estimation. There will also be a stochastic piece which varies from source to source. This will limit the precision at which χ_s can be measured, thus limiting the resolution of dispersion-space density maps in the radial direction. We note that one-point statistics from the same data set should provide empirical information about these properties independent of their physical origin.

Detailed treatment of the above source modelling is beyond the scope of this Letter. The magnitude of the contribution from the progenitor is, at present, unknown. To crudely deal with it here, we use relatively large bin widths of $\Delta\chi = 100 \text{ Mpc}/h$ and exclude the $\chi = \chi'$ bin pairs. Because the local term drops rapidly with radial separations, this effectively discards the contribution from the local term which is most sensitive to having precise radial distances.

In first measurements of the angular power spectra, uncertainty will be dominated by the finite number of observed events, or shot noise. The noise power spectrum on shells at a distance χ_i and with width $\Delta\chi$ is

$$C_{\ell,ij}^N = \frac{\delta_{ij}}{\bar{n}_f(\chi_i) \chi_i^2 \Delta\chi}. \quad (23)$$

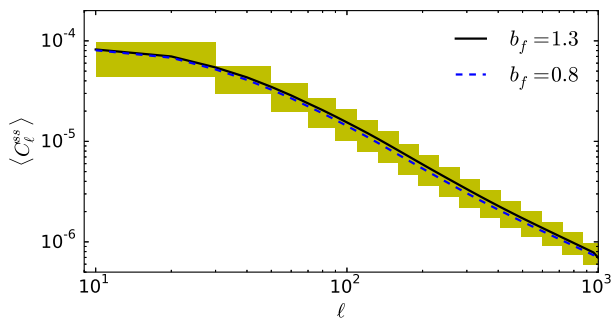


FIG. 3. Sensitivity of a survey with 10 000 dispersion measures distributed uniformly over half of the sky. Plotted is the cross-correlation power spectrum weighted averaged over all pairs of radial bins. Weights are chosen to maximize signal to noise at $\ell = 100$ for the $b_f = 1.3$ case.

Here, to indicate that we are now working with quantities binned in the radial direction, we have switched to $C_{\ell,ij}$ instead of $C_{\ell}(\chi, \chi')$. The uncertainty on the angular cross-power spectrum is then

$$(\Delta C_{\ell,ij}^{ss})^2 = \frac{1}{\ell(\ell+1)\Delta\ell f_{\text{sky}}} [C_{\ell,ii}^N C_{\ell,jj}^N + (C_{\ell,ij}^N)^2], \quad (24)$$

where the second term in brackets only contributes for $i = j$.

We consider the sensitivity of a survey with a total of 10 000 dispersion measures from FRB events distributed uniformly over half of the sky. To give an idea of the overall sensitivity of the survey, we collapse $C_{\ell,ij}^{ss}$ to a single function of ℓ by taking a weighted average of all pairs of radial bins over the range 500 Mpc/h to 3500 Mpc/h. For weights we use the signal over noise squared at $\ell = 100$, which maximizes the signal to noise at that ℓ and is near optimal at other multipoles. To determine if such a survey would be able to distinguish between models of FRB clustering we plot the same quantity for $b_f = 0.8$. The result is shown in Fig. 3.

Discussion and conclusions.—We have proposed using cosmological FRB sources as standard pings to trace the 3D large-scale structure of the Universe using dispersion distance. It can be seen in Fig. 2 that the signal is dominated by inhomogeneities in the electron density along the different lines of sight, inducing misestimates of radial distance, and thus apparent clustering. Because it is the line-of-sight integrated structure that correlates, the signal is fairly insensitive to radial distance and the radial separation of slices, with these dependencies being dominated by the coefficient $A(\chi)$. These dispersion-space distortions could be used to study the distribution of free electrons in the Universe on large scales. There have been other proposals to use FRBs for cosmology [17, 24–27]; however these schemes have either not been three dimensional or required externally measured redshifts for the sources.

We have shown in Fig. 3 that a survey detecting 10 000 fast radio bursts of cosmological origin could detect the clustering signal. This is in rough approximation to what might be

achieved in a reasonable amount of time by the Canadian Hydrogen Intensity Mapping Experiment (CHIME)¹, the Square Kilometre Array², or other upcoming wide-field telescopes. Such a survey would be primarily sensitive to the integral term and thus rather insensitive to the details of FRB clustering models. Looking forward, dispersion-space clustering could become a precision probe of large-scale structure should observational factors turn out to be favorable compared to spectroscopic surveys. The baryon acoustic oscillation feature can be clearly seen in Fig. 2 in the cross term and both local-term curves. It may also be possible to extract the baryon acoustic oscillation feature from the integral term using tomography. This, however, requires that the statistics of the contribution to dispersion from the source’s environment and host halo to be well understood or small compared to the contribution from the line of sight.

Finally, we note that alone—or in combination with redshift data on a subset of the population, independent redshift surveys, or gravitational lensing surveys—dispersion-space surveys could yield very powerful probes of cosmology. Cosmological dispersion-space data could open a new window into the structure of the Universe.

We thank Ue-Li Pen and Mathew McQuinn for helpful discussions. K.W.M is supported by the Canadian Institute for Advanced Research, Global Scholars Program. The research of K. S. is supported in part by a National Science and Engineering Research Council (NSERC) of Canada Discovery Grant.

-
- [1] D. R. Lorimer, M. Bailes, M. A. McLaughlin, D. J. Narkevic, and F. Crawford, *Science* **318**, 777 (2007), arXiv:0709.4301.
 - [2] E. F. Keane, B. W. Stappers, M. Kramer, and A. G. Lyne, *MNRAS* **425**, L71 (2012), arXiv:1206.4135 [astro-ph.SR].
 - [3] D. Thornton, B. Stappers, M. Bailes, B. Barsdell, S. Bates, N. D. R. Bhat, M. Burgay, S. Burke-Spolaor, D. J. Champion, P. Coster, N. D’Amico, A. Jameson, S. Johnston, M. Keith, M. Kramer, L. Levin, S. Milia, C. Ng, A. Possenti, and W. van Straten, *Science* **341**, 53 (2013), arXiv:1307.1628 [astro-ph.HE].
 - [4] L. G. Spitler, J. M. Cordes, J. W. T. Hessels, D. R. Lorimer, M. A. McLaughlin, S. Chatterjee, F. Crawford, J. S. Deneva, V. M. Kaspi, R. S. Wharton, B. Allen, S. Bogdanov, A. Brazier, F. Camilo, P. C. C. Freire, F. A. Jenet, C. Karako-Argaman, B. Knispel, P. Lazarus, K. J. Lee, J. van Leeuwen, R. Lynch, S. M. Ransom, P. Scholz, X. Siemens, I. H. Stairs, K. Stovall, J. K. Swiggum, A. Venkataraman, W. W. Zhu, C. Aulbert, and H. Fehrmann, *ApJ* **790**, 101 (2014), arXiv:1404.2934 [astro-ph.HE].
 - [5] S. Burke-Spolaor and K. W. Bannister, *ApJ* **792**, 19 (2014), arXiv:1407.0400 [astro-ph.HE].
 - [6] E. Petroff, M. Bailes, E. D. Barr, B. R. Barsdell, N. D. R. Bhat, F. Bian, S. Burke-Spolaor, M. Caleb, D. Champion,

¹ <http://chime.phas.ubc.ca/>

² <http://www.skatelescope.org/>

- P. Chandra, G. Da Costa, C. Delvaux, C. Flynn, N. Gehrels, J. Greiner, A. Jameson, S. Johnston, M. M. Kasliwal, E. F. Keane, S. Keller, J. Kocz, M. Kramer, G. Leloudas, D. Malesani, J. S. Mulchaey, C. Ng, E. O. Ofek, D. A. Perley, A. Possenti, B. P. Schmidt, Y. Shen, B. Stappers, P. Tisserand, W. van Straten, and C. Wolf, *MNRAS* **447**, 246 (2015), arXiv:1412.0342 [astro-ph.HE].
- [7] V. Ravi, R. M. Shannon, and A. Jameson, *ApJ* **799**, L5 (2015), arXiv:1412.1599 [astro-ph.HE].
- [8] A. Rane, D. R. Lorimer, S. D. Bates, N. McMann, M. A. McLaughlin, and K. Rajwade, *ArXiv e-prints* (2015), arXiv:1505.00834 [astro-ph.HE].
- [9] K. Dolag, B. M. Gaensler, A. M. Beck, and M. C. Beck, *MNRAS* **451**, 4277 (2015), arXiv:1412.4829.
- [10] J. Luan and P. Goldreich, *ApJ* **785**, L26 (2014), arXiv:1401.1795 [astro-ph.HE].
- [11] U.-L. Pen and L. Connor, *ApJ* **807**, 179 (2015), arXiv:1501.01341 [astro-ph.HE].
- [12] L. Connor, J. Sievers, and U.-L. Pen, *ArXiv e-prints* (2015), arXiv:1505.05535 [astro-ph.HE].
- [13] Z. Zheng, E. O. Ofek, S. R. Kulkarni, J. D. Neill, and M. Juric, *ApJ* **797**, 71 (2014), arXiv:1409.3244 [astro-ph.HE].
- [14] S. Inoue, *MNRAS* **348**, 999 (2004), astro-ph/0309364.
- [15] K. Ioka, *ApJ* **598**, L79 (2003), astro-ph/0309200.
- [16] N. Kaiser, *MNRAS* **227**, 1 (1987).
- [17] M. McQuinn, *ApJ* **780**, L33 (2014), arXiv:1309.4451 [astro-ph.CO].
- [18] D. N. Limber, *ApJ* **117**, 134 (1953).
- [19] N. Kaiser, *ApJ* **388**, 272 (1992).
- [20] N. Kaiser, *ApJ* **498**, 26 (1998), astro-ph/9610120.
- [21] M. LoVerde and N. Afshordi, *Phys. Rev. D* **78**, 123506 (2008), arXiv:0809.5112.
- [22] C. Blake, S. Brough, M. Colless, C. Contreras, W. Couch, S. Croom, T. Davis, M. J. Drinkwater, K. Forster, D. Gilbank, M. Gladders, K. Glazebrook, B. Jelliffe, R. J. Jurek, I.-H. Li, B. Madore, D. C. Martin, K. Pimbblet, G. B. Poole, M. Pracy, R. Sharp, E. Wisnioski, D. Woods, T. K. Wyder, and H. K. C. Yee, *MNRAS* **415**, 2876 (2011), arXiv:1104.2948.
- [23] P. Schechter, *ApJ* **203**, 297 (1976).
- [24] B. Dennison, *MNRAS* **443**, L11 (2014), arXiv:1403.2263 [astro-ph.HE].
- [25] W. Deng and B. Zhang, *ApJ* **783**, L35 (2014), arXiv:1401.0059 [astro-ph.HE].
- [26] B. Zhou, X. Li, T. Wang, Y.-Z. Fan, and D.-M. Wei, *Phys. Rev. D* **89**, 107303 (2014), arXiv:1401.2927.
- [27] H. Gao, Z. Li, and B. Zhang, *ApJ* **788**, 189 (2014), arXiv:1402.2498.